Applied Physics Letters

Reversible strain-induced spin–orbit torque on flexible substrate

Cite as: Appl. Phys. Lett. **119**, 042402 (2021); https://doi.org/10.1063/5.0056995
Submitted: 17 May 2021 . Accepted: 19 July 2021 . Published Online: 29 July 2021

Grayson Dao Hwee Wong, Calvin Ching Ian Ang, Weiliang Gan, Wai Cheung Law, Zhan Xu, Feng Xu, Chim Seng Seet, and Wen Siang Lew

AIP Publishing

Applied Physics Letters ARTICLE scitation.org/journal/apl

Reversible strain-induced spin–orbit torque on flexible substrate

Cite as: Appl. Phys. Lett. **119**, 042402 (2021); doi: 10.1063/5.0056995
Submitted: 17 May 2021 · Accepted: 19 July 2021 ·
Published Online: 29 July 2021

Grayson Dao Hwee Wong,[1,2] Calvin Ching Ian Ang,[1] Weiliang Gan,[1] Wai Cheung Law,[1,2] Zhan Xu,[1,3] Feng Xu,[3] Chim Seng Seet,[2] and Wen Siang Lew[1,a)]

AFFILIATIONS

[1]School of Physical and Mathematical Sciences, Nanyang Technological University, 21 Nanyang Link, Singapore 637371
[2]GLOBALFOUNDRIES Singapore Pte. Ltd., 60 Woodlands Industrial Park D St 2, Singapore 738406
[3]MIIT Key Laboratory of Advanced Metallic and Intermetallic Materials Technology, School of Materials Science and Engineering, Nanjing University of Science and Technology, Nanjing 210094, China

[a)]Author to whom correspondence should be addressed: wensiang@ntu.edu.sg

ABSTRACT

We propose the use of mechanical strain and mild annealing to achieve reversible modulation of spin–orbit torque (SOT) and Gilbert damping parameter. X-ray diffraction results show that the residual spin–orbit torque enhancement and Gilbert damping reduction, due to the post-mechanical strain treatment, can be reset using mild annealing to alleviate the internal strain. The spin Hall efficiency of the heat- and strain-treated Pt/Co bilayer was characterized through spin-torque ferromagnetic resonance, and it was found that the device could switch between the strain enhanced SOT and the pristine state. The Gilbert damping parameter behaves inversely with the spin Hall efficiency, and therefore, strain can be used to easily tune the device switching current density by a factor of ∼2 from its pristine state. Furthermore, the resonance frequency of the Pt/Co bilayer could be tuned using purely mechanical strain, and from the endurance test, the Pt/Co device can be reversibly manipulated over 10^4 cycles demonstrating its robustness as a flexible device.

The ability to manipulate magnetization has helped the current-induced spin–orbit torque (SOT) gather a considerable amount of interest in recent decades.[1–6] SOT is induced by a pure spin current that is generated as the result of a spin–orbit interaction when a charge current passes through a non-magnetic metal.[6,7] In heavy-metal/ferromagnetic (HM/FM) heterostructures, the SOT is contributed by two established phenomena: the spin Hall effect (SHE) in the HM and/or the Rashba–Edelstein effect at the HM/FM interface.[8–11] The spin Hall efficiency θ_{eff} is commonly used to quantify the performance of this charge-to-spin conversion, and it is ideal to have a large θ_{eff} for better energy-efficient memory. To date, most studies are concentrated around HM with a strong spin–orbit coupling (SOC), such as Pt, β-Ta, and β-W, topological insulators, and even antiferromagnetic materials.[12–18]

To further push the boundaries of the θ_{eff}, many efforts have been devoted to manipulating the extrinsic contribution of the spin Hall effect (SHE). Such works include alloying of the HM with lighter conductive metals, usage of insertion layers within the HM and the varying deposition condition of the HM, and many others.[19–24] The extrinsic SHE mechanism capitalizes on electron scattering caused by impurities within the HM, and the two most prominent scattering processes are skew scattering and side-jump scattering.[25,26] Although the θ_{eff} can be easily enhanced through tuning the resistivity of the HM, its manipulation after the device fabrication is irreversible.[22–24] Among them, the use of mechanical strain is a promising candidate not only for enhancing the θ_{eff} but also for tuning it reversibly.[27,28] Previous works have demonstrated SOT enhancement with the use of strain;[29] however, the ability to revert the enhancement has yet to be demonstrated and research is required to further develop the use of mechanical strain into a feasible option for the manipulation of the SOT.

In this work, we demonstrate the ability to manipulate the strain-mediated SOT enhancement reversibly in Pt/Co using a combination of mechanical strain and mild annealing. By annealing Pt/Co at mild temperatures, the internal strain induced by mechanical tensile strain is alleviated, and this has been confirmed using x-ray diffraction (XRD). When the internal strain is removed, the device behaves similarly to its pristine state making further manipulation of the device possible. The generated spin current was characterized using the spin-torque ferromagnetic resonance technique (ST-FMR), and the Gilbert

damping parameter of Pt/Co was found to behave inversely with the manipulated SOT. Furthermore, using the mechanical tensile strain, the resonance field of Pt/Co devices can be tuned allowing for microwave detection applications. These findings establish a unique technique to influence the strain-mediated SOT and have a considerable contribution to the development of flexible spintronics devices.

The effects of tensile strain and mild annealing on the spin current generation of Pt/Co bilayers are characterized using the spin-torque ferromagnetic resonance (ST-FMR) measurement. The bilayer Pt(5 nm)/Co(5 nm) films used in this study were deposited using magnetron sputtering onto unstrained flexible Kapton at room temperature using an Ar pressure of 2 mTorr and a base pressure lower than 5×10^{-8} Torr. A Ti(5 nm) seed and a cap layer were used for film adhesion and oxidation prevention, and from the previous study, it was shown that Ti does not contribute to spin current generation.[29] Within the bilayer, Pt takes up the role of the SOT generation via SHE due to its strong SOC. ST-FMR devices and coplanar waveguides (CPWs) were patterned using optical lithography. Figure 1(a) illustrates the ST-FMR measurement setup and device. During the ST-FMR measurement, a microwave radio frequency (RF) charge current (J_C) is injected into the CPW and along the longitudinal direction of the microstrip device ($10 \times 50\ \mu m^2$). Simultaneously, an in-plane external magnetic field (H_{ext}) is applied at a 45° angle with respect to the longitudinal direction of the device. The RF current passing through the Pt layer generates an oscillating transverse spin current by SHE, which will then enter the adjacent Co layer. The magnetization of the Co layer experiences an in-plane and out-of-plane torque from the RF current.[16,17] When the RF spin current frequency matches the precessional frequency of the magnetization, the FMR is established, and the oscillating torques will result in the oscillation of the device resistance due to anisotropic magnetoresistance in the Co layer. By using a bias tee, the mixing of the RF current and the oscillating resistance is measured as a rectified DC voltage signal (V_{mix}).

The magnitude of the strain ε was approximated using $\varepsilon = T/2R$, where T and R are the total thickness of the substrate ($120\ \mu m$) and the bilayer structure and the curvature radius of the

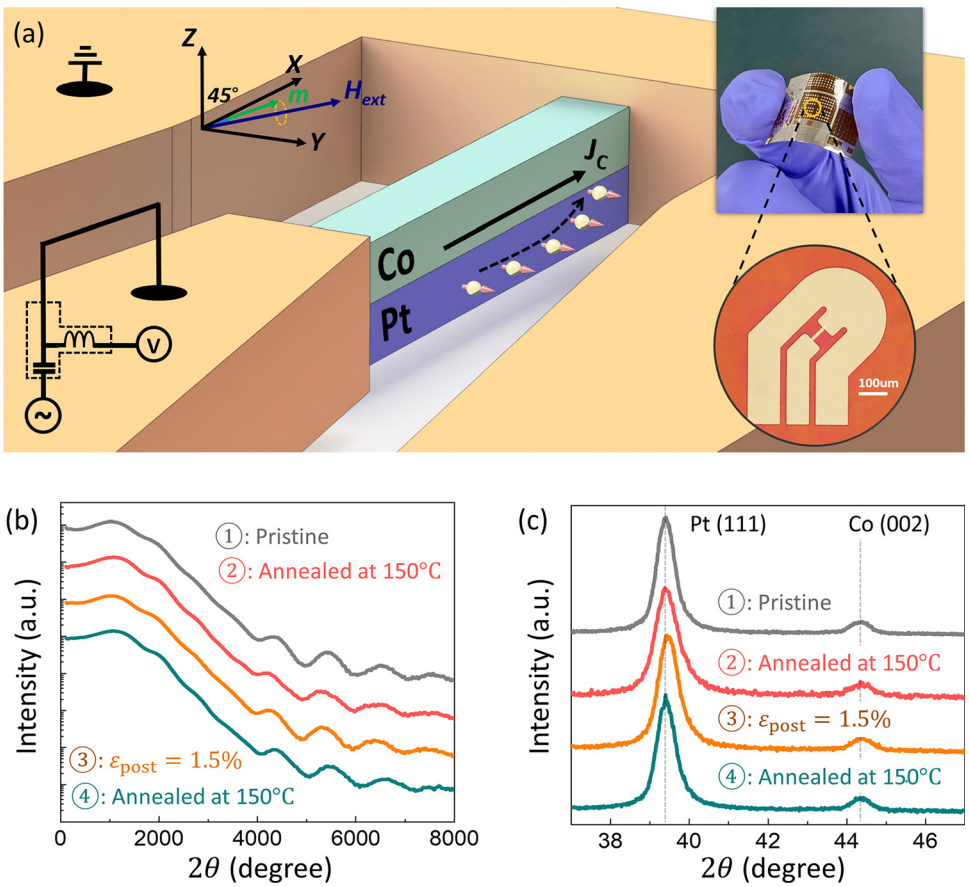

FIG. 1. (a) Schematic illustration of the Pt/Co bilayer device for the ST-FMR measurement. The green and navy blue arrows represent the precessing magnetization in the Co layer and the applied external field, respectively. An RF current was applied along the longitudinal direction (*x*-axis) of the device generating two orthogonal torques as it passes through the heavy metal. Photo of strained ST-FMR devices on the flexible Kapton substrate and the optical image of the device are as shown in the inset. (b) X-ray reflectivity profiles for Pt(5 nm)/Co(10 nm) films at different steps of the process: step ① is the pristine film, step ② is the pristine film annealed at 150 °C for 1 h, step ③ is the tensile strain treatment of $\varepsilon_{post} = 1.5\%$ for 1 h, and step ④ is the annealing process at 150 °C for 1 h. (c) X-ray diffraction spectra of Pt(25 nm)/Co(25 nm) films demonstrating a right shift in the Pt(111) peak shift when strained and back when treated with mild annealing.

mold, respectively.[30] All strains used in this work are mechanical tensile strain, and the direction of the strain is along the longitudinal direction of the microstrip. Two methods of strain measurement were used. The first is the strain treatment, where the sample is strained at a specific ε_{post} for 1 h and measured at its relaxed state, while the second is an *in situ* strain measurement where the sample is strained at ε_{in} during measurement.

X-ray reflectivity (XRR) spectroscopy was performed on Pt(5 nm)/Co(10 nm) at different steps of the characterization process to determine the effects of strain and mild annealing on the interfacial roughness between Pt and Co. The sample used throughout the different step processes is the same, and the spectra are shown in Fig. 1(b). The different steps of the process are: step ① is where the film is pristine, and this is used as a reference; step ② is the pristine film after being vacuum annealed at 150 °C for 1 h; step ③ is the annealed film treated with a tensile strain of $\varepsilon_{post} = 1.5\%$ for 1 h; and step ④ is the strain-treated film after annealing at 150 °C for 1 h. From the XRR measurements (see the supplementary material), no significant change in interfacial roughness was observed, and this concurs with previous study that the strain-mediated SOT enhancement is a bulk effect due to the extrinsic SHE.[29,31] X-ray diffraction measurement was also performed on Pt(25 nm)/Co(25 nm) films for steps ①, ②, ③, and ④. Similar to the XRR measurement, the XRD sample used for all four steps is the same. From Fig. 1(c), the Pt(111) peak shifts right after the strain treatment indicating that the internal strain persists within the film even after the strain has been removed. However, upon treating the film with mild annealing, the Pt(111) peak shifted back. This demonstrates the use of annealing as a means to relieve the residual internal strain-induced and suggests that the strain-mediated SOT enhancement can be reversed. Unlike the Pt(111) peak, the Co(002) peak remains stationary, and this difference in response found in the Co and Pt layers is due to their different Poison's ratios.[32] This implies that the Co layer is unaffected by both the strain and mild annealing.

Figure 2(a) shows the ST-FMR spectra for bilayer Pt/Co measured at a microwave power of 12 dBm with a frequency range of 8–17 GHz in steps of 1 GHz. The measured V_{mix} consists of a symmetric and anti-symmetric Lorentzian function, which can be expressed as

$$V_{mix} = V_0[SF_S(H_{ext}) + AF_A(H_{ext})], \quad (1)$$

where

$$V_0 = -\frac{1}{4}\frac{dR}{d\varphi}\frac{\gamma\mu_0 I_{RF}\cos\varphi}{2\pi\Delta H(df/dH_{ext})|_{H_{ext}=H_{res}}},$$

$$F_S(H_{ext}) = \frac{\Delta H^2}{(H_{ext}-H_{res})^2+\Delta H^2},$$

and

$$F_A(H_{ext}) = \frac{\Delta H(H_{ext}-H_{res})}{(H_{ext}-H_{res})^2+\Delta H^2}.$$

Here, V_0, ΔH, H_{ext}, S, and A are the scaling factors, linewidth, the applied external field, the magnitude of the symmetric and anti-symmetric components of the V_{mix}, respectively. The symmetric component is proportional to the damping-like torque, and the anti-symmetric component is the result of the sum of the Oersted field and the field-like torque.[16,33] The peak-to-peak voltage V_{P-P} of the

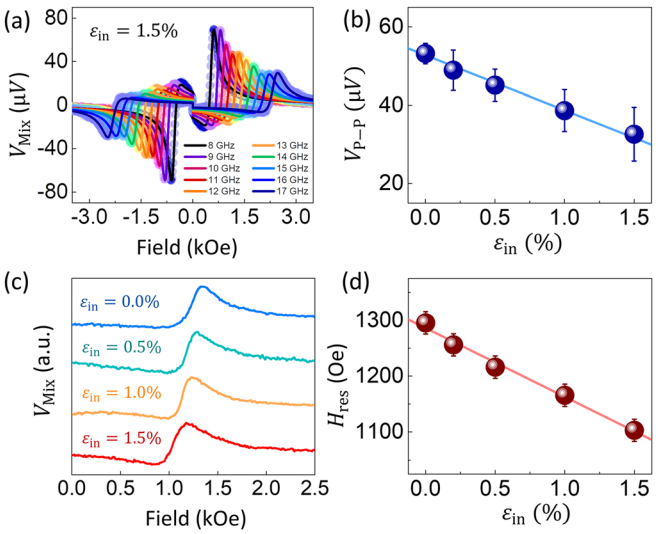

FIG. 2. (a) Measured ST-FMR spectra of the Pt/Co bilayer while applying $\varepsilon_{in} = 1.5\%$ for frequencies between 8 and 17 GHz using a microwave power of 12 dBm. (b) *In situ* strain dependence of V_{P-P} measured at 12 GHz. (c) Leftward shift of ST-FMR spectra due to the tensile strain at varying ε_{in}. (d) *In situ* strain dependence of H_{Res}.

ST-FMR spectra decreases with increasing ε_{in} as shown in Fig. 2(b). From Eq. (1), there are several contributing factors such as ΔH, and $(df/dH_{ext})|_{H_{ext}=H_{res}}$ can lead to a change in V_{P-P}. However, the magnitude of V_{P-P} is primarily influenced by the resistivity of Pt as an increased resistivity would decrease the current density through the Pt layer. When the tensile strain is employed along the longitudinal direction of the microstrip, the strip elongates and narrows along the direction of strain resulting in an enhancement in resistivity.

To determine the change in Pt resistivity, a separate set of single layer Pt(5 nm) microstrips were fabricated and characterized using a semiconductor analyzer at different steps as shown in Fig. 3(a). At step ①, the film is in its pristine state after fabrication. To set the device, the sample is annealed at 150 °C for 1 h in step ②. The resistivity slightly decreased as a result of the improvement in film quality from the mild annealing. Thereafter in step ③, a tensile strain of $\varepsilon_{post} = 1.5\%$ was applied for 1 h. During the strain treatment, the resistivity increases as the microstrips are stretched along the longitudinal direction, resulting in a narrower cross-sectional area. Relaxing the film after the treatment for measurement, the residual strain within the Pt retains the enhanced resistivity as shown in the plot. For step ④, the sample was annealed at 150 °C for 1 h before characterization, and upon mild annealing, the resistivity of Pt decreases as the internal strain caused by the strain treatment is relieved. Finally, steps ⑤ and ⑥ are repeated steps that are the same as steps ③ and ④, respectively, that show the repeatability of the process. The strain response of Co resistivity was measured and found to be negligible in contrast to Pt (refer to the supplementary material).

Since the Pt layer thickness is much larger than its spin diffusion length, the field-like torque in bilayer Pt/Co can be assumed to be negligibly small as shown in previous work.[16,29,34] Using this approximation, the spin Hall efficiency for the Pt/Co bilayer is calculated by the following expression:

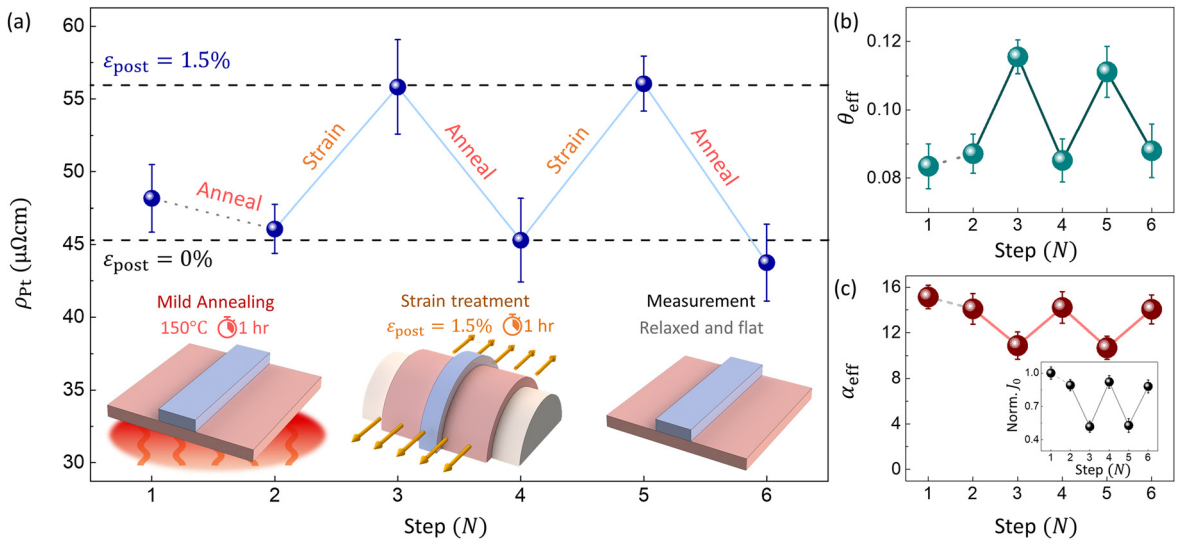

FIG. 3. (a) Resistivity of a single layer Pt(5 nm) microstrip measured at different steps of N with the inset illustrating the individual steps: step ① is the pristine film, step ② is the pristine film annealed at 150 °C for 1 h, step ③ is the annealed film treated with a tensile strain of $\varepsilon_{post} = 1.5\%$ for 1 h, step ④ is the strain-treated film annealed at 150 °C for 1 h, and steps ⑤ and ⑥ are repeated treatment procedures that are the same as steps ③ and ④, respectively. (b) From the ST-FMR measurements of the Pt/Co bilayer, θ_{eff} and (c) Gilbert damping parameter as a function of N are presented. The normalized switching current density of the Pt/Co bilayer is shown in the inset.

$$\theta_{eff} = \frac{S}{A}\frac{e\mu_0 M_S t_{Co} t_{Pt}}{\hbar}\sqrt{1+\frac{4\pi M_{eff}}{H_{res}}}, \tag{2}$$

where t_{Co} and t_{Pt} are the thicknesses of Co and Pt layers, respectively, M_S is the magnetization saturation, and M_{eff} is the effective magnetization. The M_S of bilayer Pt/Co measured at $\varepsilon_{post} = 0\%$ and 1.5% was obtained to be 1220±30 and 1130±40 emu/cc^3, respectively, which is within a range consistent with other works, and therefore, the magnetic proximity effect is assumed to be negligible in this study.[35–38] To obtain the required M_{eff}, the in-plane magnetization Kittel equation $f = \gamma/2\pi\sqrt{(H_{res}+H_K)(4\pi M_{eff}+H_{res}+H_K)}$ was used, where γ is the gyromagnetic ratio and H_K is the total magnetic anisotropy field. Having similar behavior as the ρ_{Pt}, the θ_{eff} at various measurement steps is as summarized in Fig. 3(b). From the proportionality between both the ρ_{Pt} and θ_{eff}, the strain-mediated SOT enhancement is a result of the extrinsic SHE in the Pt layer.

Predominantly, the ΔH of the ST-FMR spectra is broadened by extrinsic contribution such as the film inhomogeneous broadening term (ΔH) and two magnon scattering. Two magnon scattering results in a nonlinear frequency dependence of the ΔH, which is not observed in the measured samples.[39] The effective Gilbert damping parameter (α_{eff}) was calculated from the ΔH dependences of the frequency expressed as $\Delta H = \Delta H_0 + 4\pi f \alpha_{eff}/\gamma$, where ΔH is a result of sample imperfections that are assumed to be frequency independent, and the data are as shown in Fig. 3(c). The two main α_{eff} contributors of bilayer Pt/Co are the intrinsic Gilbert damping (α_{int}) from Co and the damping introduced by the spin pumping effect (α_{SP}) due to the adjacent Pt.[40,41] α_{int} remains unchanged as it is independent of the strain-induced magnetic anisotropy.[42–44] The α_{SP}, however, is highly dependent on the spin pumping effect at the interface between the Pt and Co layers. An enhancement in the extrinsic SHE will result in a greater spin pumping effect and, hence, larger α_{SP} contribution. Therefore, α_{eff} has an inverse trend as compared to the ρ_{Pt} and θ_{eff}.

The effects of strain and mild annealing on the critical switching current density J_{C0} of an in-plane magnetization SOT device can be evaluated using the following equation:

$$J_{C0} \approx \frac{2e}{\hbar}\frac{\alpha_{eff}}{\theta_{eff}}\left(\frac{4\pi M_{eff}}{2}\right)M_S t_{FM}. \tag{3}$$

From this equation, J_{C0} is proportional to the ratio $\alpha_{eff}/\theta_{eff}$, and a decrease in this ratio will denote a lower J_{C0}.[35,45] The inset in Fig. 3(c) shows how the J_{C0} can be controlled using a combination of mechanical strain and mild annealing. This method allows the J_{C0} to alternate between ~90% and ~50% of the pristine J_{C0}, allowing for an additional degree of freedom in inducing magnetization reversal of the SOT device.

Aside from SOT manipulation, the mechanical strain can also be used to tune the resonance frequency by shifting the FMR spectrum, and from Fig. 2(c), a left shift motion of the ST-FMR spectra is observed as the *in situ* tensile strain applied increases.[46] The shift in H_{Res} is attributed by the magnetoelastic anisotropy induced by the mechanical tensile strain. This additional anisotropy has an easy axis perpendicular to the uniaxial anisotropy generated by the external magnetic field, which will result in a shift in the magnetic easy axis of the Pt/Co bilayer.[30] Figure 2(d) shows the H_{Res} dependence of ε_{in}. The Pt/Co device has a tunable H_{Res} with a magnitude of −123±6 Oe per unit ε_{in}. Using this tuning capability, the detectable H_{Res} can be adjusted based on the applied strain and then reversed by relaxing the device.

Figure 4(a) demonstrates how the Pt/Co device can switch between two states of H_{Res} by applying strain and relaxing it. The first cycle begins with the device in the pristine state measured at the relaxed position. Subsequently, the even cycles refer to the *in situ* strain device while the odd cycles are measured when the device is relaxed. With every cycle, a distinct shift in H_{Res} is observed. This cycle of

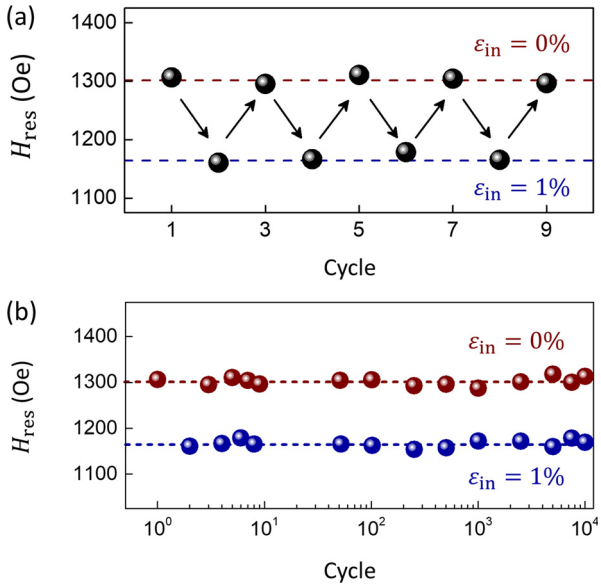

FIG. 4. (a) H_{Res} of the Pt/Co bilayer as a function of the reversible tensile strain $\varepsilon_{in} = 0\%$ and $\varepsilon_{in} = 1\%$ performed using a microwave frequency of 12 GHz. (b) H_{Res} over 10 000 cycles of bending and relaxing to demonstrate the robustness of the device.

straining and relaxing is performed continuously for a repeatability test as shown in Fig. 4(b). For consistency of the cycles, the straining and relaxing are performed using a linear actuator attached with a stepper motor. The H_{Res} at both 0% and 1% strain are highly stable for 10^4 cycles demonstrating the device robustness against the mechanical strain.

In summary, we investigated the use of mild annealing and mechanical strain for reversible manipulation of the SOT. In the Pt/Co bilayer, XRD spectra show that the tensile strain induces a residual strain within the Pt layer that can be alleviated by treating the film with mild annealing. Using a combination of these two treatment methods, the spin Hall efficiency and Gilbert damping parameter become versatile and can be tuned with ease even after fabrication. Apart from SOT manipulation, strain can be used to tune the resonance field of the Pt/Co bilayer, and in the endurance test performed, the tunability of the device remains highly stable even after 10^4 cycles. These results pave an alternative avenue for manipulating the SOT reversibly that can also be used as a tunable microwave detector.

See the supplementary material for the interfacial roughness of the Pt and Co layers measured using XRR and the Co resistivity change at different N steps.

AUTHORS' CONTRIBUTIONS

G.D.H.W. conceived the idea, designed this work, drafted the manuscript, and fabricated the devices for measurement. W.C.L. assisted in the development of the experimental setup. W.L.G., C.C.I.A., and Z.X. made scientific comments on the result. W.S.L., C.S.S., and F.X. coordinated and supervised the entire work. All authors contributed to the discussion and the revision of the final manuscript.

This work was supported by an Industry-IHL Partnership Program (No. NRF2015-IIP001-001) and an EDB-IPP (Grant No. RCA-17/284). This work was also supported by the RIE2020 ASTAR AME IAF-ICP Grant No. I1801E0030.

The authors declare that they have no competing interest.

DATA AVAILABILITY

The data that support the findings of this study are available within the article and its supplementary material. The data that support the findings of this study are available from the corresponding author upon reasonable request.

REFERENCES

[1]Y. K. Kato, R. C. Myers, A. C. Gossard, and D. D. Awschalom, Science **306**, 1910–1913 (2004).
[2]J. Wunderlich, B. Kaestner, J. Sinova, and T. Jungwirth, Phys. Rev. Lett. **94**, 047204 (2005).
[3]G.-Y. Guo, S. Murakami, T.-W. Chen, and N. Nagaosa, Phys. Rev. Lett. **100**, 096401 (2008).
[4]E. Saitoh, M. Ueda, H. Miyajima, and G. Tatara, Appl. Phys. Lett. **88**, 182509 (2006).
[5]T. Kimura, Y. Otani, T. Sato, S. Takahashi, and S. Maekawa, Phys. Rev. Lett. **98**, 156601 (2007).
[6]T. Tanaka, H. Kontani, M. Naito, T. Naito, D. S. Hirashima, K. Yamada, and J. Inoue, Phys. Rev. B **77**, 165117 (2008).
[7]M. Morota, Y. Niimi, K. Ohnishi, D. Wei, T. Tanaka, H. Kontani, T. Kimura, and Y. Otani, Phys. Rev. B **83**, 174405 (2011).
[8]S. Emori, U. Bauer, S.-M. Ahn, E. Martinez, and G. S. Beach, Nat. Mater. **12**, 611–616 (2013).
[9]S. Valenzuela and M. Tinkham, J. Appl. Phys. **101**, 09B103 (2007).
[10]J. Hirsch, Phys. Rev. Lett. **83**, 1834 (1999).
[11]S. Zhang, Phys. Rev. Lett. **85**, 393 (2000).
[12]A. Mellnik, J. Lee, A. Richardella, J. Grab, P. Mintun, M. H. Fischer, A. Vaezi, A. Manchon, E.-A. Kim, and N. Samarth, Nature **511**, 449–451 (2014).
[13]J. Zhou, X. Wang, Y. Liu, J. Yu, H. Fu, L. Liu, S. Chen, J. Deng, W. Lin, and X. Shu, Sci. Adv. **5**, eaau6696 (2019).
[14]W. Zhang, W. Han, S.-H. Yang, Y. Sun, Y. Zhang, B. Yan, and S. S. Parkin, Sci. Adv. **2**, e1600759 (2016).
[15]X. Tao, Q. Liu, B. Miao, R. Yu, Z. Feng, L. Sun, B. You, J. Du, K. Chen, and S. Zhang, Sci. Adv. **4**, eaat1670 (2018).
[16]L. Liu, T. Moriyama, D. Ralph, and R. Buhrman, Phys. Rev. Lett. **106**, 036601 (2011).
[17]L. Liu, C.-F. Pai, Y. Li, H. Tseng, D. Ralph, and R. Buhrman, Science **336**, 555–558 (2012).
[18]C.-F. Pai, L. Liu, Y. Li, H. Tseng, D. Ralph, and R. Buhrman, Appl. Phys. Lett. **101**, 122404 (2012).
[19]Z. Xu, G. D. H. Wong, J. Tang, E. Liu, W. Gan, F. Xu, and W. S. Lew, ACS Appl. Mater. Interfaces **12**, 32898–32904 (2020).
[20]L. Zhu and R. Buhrman, Phys. Rev. Appl. **12**, 051002 (2019).
[21]A. Fert and P. M. Levy, Phys. Rev. Lett. **106**, 157208 (2011).
[22]R. Ramaswamy, Y. Wang, M. Elyasi, M. Motapothula, T. Venkatesan, X. Qiu, and H. Yang, Phys. Rev. Appl. **8**, 024034 (2017).
[23]G. Wong, W. Law, F. Tan, W. Gan, C. Ang, Z. Xu, C. Seet, and W. Lew, Sci. Rep. **10**, 9631 (2020).
[24]J. W. Lee, Y.-W. Oh, S.-Y. Park, A. I. Figueroa, G. Van Der Laan, G. Go, K.-J. Lee, and B.-G. Park, Phys. Rev. B **96**, 064405 (2017).
[25]J. Smit, Physica **24**, 39–51 (1958).
[26]L. Berger, Phys. Rev. B **2**, 4559 (1970).
[27]M. Filianina, J.-P. Hanke, K. Lee, D.-S. Han, S. Jaiswal, A. Rajan, G. Jakob, Y. Mokrousov, and M. Kläui, Phys. Rev. Lett. **124**, 217701 (2020).
[28]E. Liu, T. Fache, D. Cespedes-Berrocal, Z. Zhang, S. Petit-Watelot, S. Mangin, F. Xu, and J.-C. Rojas-Sánchez, Phys. Rev. Appl. **12**, 044074 (2019).
[29]G. D. H. Wong, Z. Xu, W. Gan, C. C. I. Ang, W. C. Law, J. Tang, W. Zhang, P. K. J. Wong, X. Yu, F. Xu, A. T. S. Wee, C. S. Seet, and W. S. Lew, ACS Nano **15**, 8319–8327 (2021).

[30]Z. Zhang, E. Liu, W. Zhang, P. K. J. Wong, Z. Xu, F. Hu, X. Li, J. Tang, A. T. S. Wee, and F. Xu, ACS Appl. Mater. Interfaces **11**, 8258–8265 (2019).
[31]H. An, S. Haku, Y. Kanno, H. Nakayama, H. Maki, J. Shi, and K. Ando, Phys. Rev. Appl. **9**, 064016 (2018).
[32]M. De Jong, W. Chen, T. Angsten, A. Jain, R. Notestine, A. Gamst, M. Sluiter, C. K. Ande, S. Van Der Zwaag, and J. J. Plata, Sci. Data **2**, 150009 (2015).
[33]C.-F. Pai, Y. Ou, L. H. Vilela-Leão, D. Ralph, and R. Buhrman, Phys. Rev. B **92**, 064426 (2015).
[34]W. Skowroński, Ł. Karwacki, S. Ziętek, J. Kanak, S. Łazarski, K. Grochot, T. Stobiecki, P. Kuświk, F. Stobiecki, and J. Barnaś, Phys. Rev. Appl. **11**, 024039 (2019).
[35]L. Huang, S. He, Q. J. Yap, and S. T. Lim, Appl. Phys. Lett. **113**, 022402 (2018).
[36]H. Bouloussa, R. Ramaswamy, Y. Roussigné, A. Stashkevich, H. Yang, M. Belmeguenai, and S. Chérif, J. Phys. D **52**, 055001 (2019).
[37]L. Zhu, D. Ralph, and R. Buhrman, Phys. Rev. B **98**, 134406 (2018).
[38]J. Geissler, E. Goering, M. Justen, F. Weigand, G. Schütz, J. Langer, D. Schmitz, H. Maletta, and R. Mattheis, Phys. Rev. B **65**, 020405 (2001).
[39]R. Arias and D. Mills, Phys. Rev. B **60**, 7395 (1999).
[40]O. Mosendz, V. Vlaminck, J. Pearson, F. Fradin, G. Bauer, S. Bader, and A. Hoffmann, Phys. Rev. B **82**, 214403 (2010).
[41]J. M. Shaw, H. T. Nembach, and T. J. Silva, Phys. Rev. B **85**, 054412 (2012).
[42]M. Tang, W. Li, Y. Ren, Z. Zhang, and Q. Jin, J. Magn. Magn. Mater. **428**, 269–273 (2017).
[43]M. Tang, W. Li, Y. Ren, Z. Zhang, S. Lou, and Q. Jin, RSC Adv. **7**, 5315–5321 (2017).
[44]A. Barman, S. Wang, O. Hellwig, A. Berger, E. E. Fullerton, and H. Schmidt, J. Appl. Phys. **101**, 09D102 (2007).
[45]K.-S. Lee, S.-W. Lee, B.-C. Min, and K.-J. Lee, Appl. Phys. Lett. **102**, 112410 (2013).
[46]W. Liu, M. Liu, R. Ma, R. Zhang, W. Zhang, D. Yu, Q. Wang, J. Wang, and H. Wang, Adv. Funct. Mater. **28**, 1705928 (2018).